IOPscience iopscience.iop.org

Home Search Collections Journals About Contact us My IOPscience

Thermodynamics and complexity of simple transport phenomena

This article has been downloaded from IOPscience. Please scroll down to see the full text article.

2006 J. Phys. A: Math. Gen. 39 1311

(http://iopscience.iop.org/0305-4470/39/6/007)

View the table of contents for this issue, or go to the journal homepage for more

Download details:
IP Address: 171.66.16.108
The article was downloaded on 03/06/2010 at 04:59

Please note that terms and conditions apply.

INSTITUTE OF PHYSICS PUBLISHING JOURNAL OF PHYSICS A: MATHEMATICAL AND GENERAL

J. Phys. A: Math. Gen. **39** (2006) 1311–1338 doi:10.1088/0305-4470/39/6/007

Thermodynamics and complexity of simple transport phenomena

Owen G Jepps[1] **and Lamberto Rondoni**[2]

[1] Dipartimento di Matematica, Politecnico di Torino, Corso Duca degli Abruzzi 24, 10129 Torino, Italy
[2] Dipartimento di Matematica and INFM, Politecnico di Torino, Corso Duca degli Abruzzi 24, 10129 Torino, Italy

E-mail: jepps@calvino.polito.it and lamberto.rondoni@polito.it

Received 19 July 2005, in final form 22 December 2005
Published 25 January 2006
Online at stacks.iop.org/JPhysA/39/1311

Abstract

We examine the transport behaviour of non-interacting particles in a simple channel billiard, at equilibrium and in the presence of an external field. We observe a range of sub-diffusive, diffusive and super-diffusive transport behaviours. We find nonequilibrium transport that is inconsistent with the equilibrium behaviour, indicating that a linear regime does not exist for this system. However, we define a 'weak' linear regime that may lead to consistency between the equilibrium and nonequilibrium results. Despite the non-chaotic nature of the dynamics, we observe greater unpredictability (complexity) in the transport properties than is observed for chaotic systems. This observation seems at odds with existing complexity measures, motivating some new measures that attribute importance to the collective behaviour, rather than to the behaviour of individual system components. Such measures provide a new key for characterizing complexity in real-world phenomena.

PACS numbers: 05.20.−y, 05.60.−k, 05.90.+m, 89.75.−k

1. Introduction

One of the fundamental aims of statistical mechanics is to shed light upon the relationship between the macroscopic properties of a system and its underlying microscopic behaviour. In the development of such a relationship, conditions of 'molecular chaos' on the nature of the microscopic dynamics play a crucial role. The nature of such conditions is a subject of ongoing research in theories of nonequilibrium systems.

For equilibrium systems, the assumption that a system is *ergodic*—the ergodic hypothesis (EH)—allows one to associate the system's macroscopic, thermodynamic properties with its microscopic, mechanical properties. However, ergodicity is notoriously difficult to prove and is

 © 2006 IOP Publishing Ltd Printed in the UK

known to be violated in many cases of physical interest. Despite this, ergodicity is still assumed for the purpose of extracting macroscopic information from microscopic models, largely on the basis that thermodynamic data thus generated appear consistent with observations of real physical systems. At present there is a wide body of results on the applicability of the EH, and theoretical explanations of why it should work have been available for quite some time [1, 2].

In the literature of nonequilibrium systems, conditions of molecular chaos are present in the form of various 'chaotic hypotheses' (CH), which have been made either explicitly or implicitly (see, e.g., [3, 4]). In contrast with the EH, the CH are not thoroughly understood yet, and the question of how much 'molecular chaos' is sufficient to explain the observed macroscopic behaviour remains elusive [5]. For instance, recent results indicate that *thermodynamic-like* connections between the microscopic and macroscopic nature of a particle system can be forged for weaker-than-chaotic dynamical systems. In particular, behaviours reminiscent of normal diffusion and heat conduction have been observed in polygonal billiards [6, 7], where the dynamics is not chaotic. There are various numerical and mathematical works on the ergodic, mixing and transport properties of irrational polygons, see, for instance [6–13]. However, the models are limited in number, the triangular billiards being the most studied models, and many questions concerning them remain open. Despite the vanishing topological entropy of polygonal channels, pairs of orbits almost always separate [14]. Consequently, these systems exhibit a certain sensitive dependence on the initial conditions, and their dynamics may appear highly disordered, indistinguishable to the eye from chaotic motions. However, such non-chaotic dynamics would represent an extremely weak condition on the required molecular chaos.

Diffusive behaviour has also been observed in non-chaotic one-dimensional lattices of maps, and in the Ehrenfest wind-tree model[3], with spatial quenched disorder [15, 16]. Furthermore, the Gallavotti–Cohen fluctuation theorem, which invokes a 'chaotic hypothesis' [3], has been verified over an initial diffusive phase of transport in a nonequilibrium version of the periodic Ehrenfest wind-tree model [17], and in a model of a mechanical 'pump', with flat sides [18].

If these results are indicative of thermodynamic connections between microscopic and macroscopic behaviour, in systems that do not exhibit chaotic behaviour, then they implicitly call into question the nature of current chaotic hypotheses. It is, therefore, of interest to explore such non-defocusing systems in greater detail, in order to understand more deeply the nature of such apparently thermodynamic behaviour. In addition to these more fundamental issues, there is also the practical consideration of the study of transport in porous media. In certain applications of porous media, such as gas separation and storage, or the controlled delivery of pharmaceuticals, the accommodation coefficient (indicating the degree of momentum exchange between fluid molecules and the pore wall) can be exceedingly low. Consequently, over finite times (and finite pore lengths), the transport behaviour in such a pore should be well approximated by the behaviour in polygonal channels. Furthermore, in systems where the molecular size is of the same order as the pore width, the transport behaviour is dominated by solid–fluid interactions at laboratory temperatures and pressures [19]. In this respect, the systems studied in this paper resemble transport in microporous membranes at low (but practically relevant) densities, where interactions are rare.

In this paper, we consider the equilibrium and nonequilibrium mass transport of point particles in a simple two-dimensional polygonal channel, described in section 2. We examine the average transport behaviour of particles in the channel, in particular the diffusive

[3] This is one kind of polygonal billiard, with one point particle which moves in the two-dimensional plane, and undergoes elastic collisions with scatterers which have flat sides. Such collisions do not defocus neighbouring trajectories, hence chaos is absent.

behaviour, as outlined in section 3. Despite being arguably the simplest particle system that could be conceived, we observe (in section 4) a surprising array of transport behaviours. While certain properties of the system demonstrate almost trivial behaviour, other properties display an unpredictable richness, which can be expressed through a sensitive dependence of the macroscopic behaviour on the parameters which define the boundary geometry. We observe transport behaviour, which can be sub-diffusive, super-diffusive, or apparently diffusive (without excluding the possibility of a $\ln t$ tail [20]) and which depends strongly on the boundary geometry. We find that apparently diffusive behaviour is straightforward to obtain, despite the absence of chaos (in the sense of positive Lyapunov exponents) and the absence of quenched disorder. However, for those systems that are apparently diffusive at equilibrium, we fail to observe a linear regime in the nonequilibrium behaviour. These results suggest a lack of fundamentally thermodynamic behaviour, both in the dependence on the geometry of the transport law, and the lack of a linear response. Whilst the system may display ostensibly thermodynamic behaviour, this thermodynamic relationship does not bear closer scrutiny.

In our view, the dependence of the mass transport on the geometry of the system characterizes such transport as '*complex*'. Notions of complexity of billiards dynamics, based on symbolic dynamics, are commonly considered [21, 22]. Using these measures, chaotic systems would be considered much more complex than non-chaotic systems—whereas the 'symbolic richness' of a chaotic system grows exponentially in time, non-chaotic systems exhibit sub-exponential growth [21]. These measures represent unpredictability at a microscopic viewpoint. However, from the macroscopic perspective, the non-chaotic systems show a much greater diversity, and hence unpredictability, in their behaviour as a function of system parameters. While the variation of transport properties with system parameters is known to be irregular in certain chaotic systems [23–27], the mass transport law in chaotic systems is usually diffusive in nature (importantly, the irregular behaviour does not necessarily prevent a linear regime, close to equilibrium [28–30]). For the non-chaotic systems we examine, we observe an additional degree of unpredictability regarding the nature of the transport law itself. This result would seem to indicate that non-chaotic systems should be *more* complex than chaotic systems, a conclusion which sits at odds with the microscopic measures of complexity.

The difficulty here is that, while complexity is commonly characterized at the microscopic level, it is at the macroscopic level that complex behaviour manifests itself. This is true of a wide range of phenomena: in transport phenomena ranging from polymer dynamics to traffic flow; in critical phenomena such as percolation and glass transitions; and self-organizing systems in general. In particular, it is true of perhaps the most complex system known to man—the human brain. In all of these cases, the relevant complexity is not that of the elements comprising the system (which are often straightforward, if not trivial, to describe), but that of the overall behaviour. It is also the case in the transport system we examine in this paper.

In the face of these observations, we introduce in section 5 a simple set of quantities which reflect the unpredictability of a system at the *macroscopic* level. Rather than considering the complexity of the microscopic dynamics for one given set of parameters, our approach focuses on the variation of global properties—in our case, the mass transport —as a function of system parameters. Our definitions attribute a higher complexity to systems displaying a richer variety of global behaviours and not just to those whose microscopic dynamics is more chaotic. For instance, they could be directly applied to characterize complexity in polymer systems which are not completely understood, such as in the coil–globule transition in confined polymer chains [31]. Here, the gyration radius scaling laws vary discontinuously with system parameters (temperature), even though the underlying dynamics varies continuously. This

distinction between macroscopic and microscopic complexities seems to be a key to a proper understanding and characterization of the 'complexity' of real-world phenomena, in which the macroscopic aspects are much more relevant to the behaviour than the microscopic ones.

2. System details

Let us begin by giving an outline of the dynamical system we shall consider in this paper and the simulation methodology. We recall the notion of a polygonal billiard.

Definition 1. *Let $\mathcal{P}$ be a bounded domain in the Euclidean plane $\mathbb{R}^2$ or on the standard torus $\boldsymbol{T}^2$, whose boundary $\partial\mathcal{P}$ consists of a finite number of (straight) line segments. A polygonal billiard is a dynamical system generated by the motion of a point particle with constant unit speed inside $\mathcal{P}$ and with elastic reflections at the boundary $\partial\mathcal{P}$.*

As usual, elastic reflection implies that the angle of incidence and angle of reflection are equal for the reflected particle, so that the reflection can also be described as 'specular'. In the general theory of polygonal billiards, $\mathcal{P}$ is not required to be convex or simply connected; the boundary may contain internal walls. If the trajectory hits a corner of $\mathcal{P}$, in general it does not have a unique continuation, and thus it normally stops there.

In continuous time, the dynamics are represented by a flow $\{S^t\}_{t\in(-\infty,\infty)}$ in the phase space $\mathcal{M} = \mathcal{P} \times \boldsymbol{T}^1$, where $\boldsymbol{T}^1$ is the unit circle of the velocity angles ϑ. Because the dynamics are Hamiltonian, the flow preserves the standard measure $\mathrm{d}x\,\mathrm{d}y\,\mathrm{d}\vartheta$ (with $(x, y) \in \mathbb{R}^2$ or $\boldsymbol{T}^2$, such that $(x, y) \in \mathcal{P}$). In discrete time, the dynamics are represented by the 'billiard map' ϕ, on the phase space $\Phi = \{(q, v) \in \mathcal{M} : q \in \partial\mathcal{P}, \langle v, n(q)\rangle \geqslant 0\}$ where $n(q)$ is the inward normal vector to $\partial\mathcal{P}$ at q and $\langle\cdot,\cdot\rangle$ is the scalar product. Therefore, ϕ is the first return map, and the ϕ-invariant measure on Φ induced by $\mathrm{d}x\,\mathrm{d}y\,\mathrm{d}\vartheta$ is $\sin\vartheta\,\mathrm{d}\vartheta\,\mathrm{d}s$, if s is the arclength on $\partial\mathcal{P}$. Unfortunately, these standard measures are not necessarily selected by the dynamics, in the sense that different absolutely continuous measures are not necessarily evolved towards them. This weakens considerably the importance of the standard measures in the case of non-ergodic polygons.

Definition 2. *A polygon $\mathcal{P}$ is called* rational *if the angles between its sides are of the form $\pi m/n$, where m, n are integers. It is called irrational otherwise.*

While polygonal billiards are easily described, their dynamics are extremely difficult to characterize. For instance, it is known that rational polygons are not ergodic and that they possess periodic orbits. But it is not known whether generic irrational polygons have any periodic orbit. On the other hand, it is known that irrational polygons whose angles admit a certain superexponentially fast rational approximation are ergodic [10]. In particular, the ergodic polygonal billiards are a dense G_δ set[4] in any compact set $\mathcal{Q}$ of polygons with a fixed number of sides, such that the rational polygons with angles with arbitrarily large denominators are dense in $\mathcal{Q}$ [32]. It is not the purpose of this paper to review exhaustively the properties of polygonal billiards, therefore we refer to the cited literature for further details.

The special class of polygons that we consider consists of channels that are periodic in the x direction, but bounded by walls in the y direction. The walls consist of straight edges and are arranged in a saw-tooth configuration such that the top and bottom walls are 'in phase', i.e. the peaks of the upper and lower walls have the same horizontal coordinate. The channel can therefore be represented as an elementary cell (EC), as depicted in figure 1,

[4] A subset Y of a compact metric space X is a dense G_δ set of X, if Y is a countable intersection of dense open subsets of X.

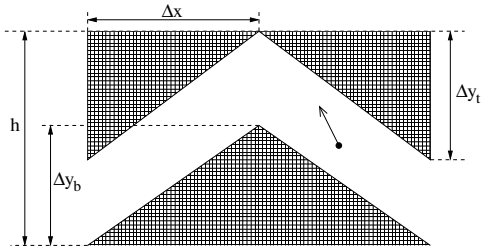

Figure 1. Elementary cell of the symmetric saw-tooth pore model used throughout this paper. The total pore height is denoted by h. The 'tooth' heights on the top and bottom are denoted by Δy_t and Δy_b, respectively, and both have length Δx. The length of the unit cell, which is repeated periodically in the x direction, is $2\Delta x = 1$.

replicated along the x-axis. We denote by h the height of this cell[5]. The heights of the isosceles triangles comprising the 'teeth' along the top and bottom cell walls are denoted by Δy_t and Δy_b, respectively, and their lengths in the x direction are denoted by Δx. The EC has unit length, so that $2\Delta x = 1$. We also introduce the mean interior channel height d, defined as $d = h - (\Delta y_t + \Delta y_b)/2$, which is equal to the mean height of the pore volume accessible to particles inside the channel. For convenience, we introduce the angles

$$\theta_i = \tan^{-1}\left(\frac{\Delta y_i}{\Delta x}\right), \qquad \text{for} \quad i = b, t. \tag{1}$$

In this paper, we consider a range of values of h, Δy_t and Δy_b, which can be classified into two groups. First, we consider systems where $\Delta y_t = \Delta y_b$ (and consequently $\theta_t = \theta_b$). In this case, the top and bottom saw-teeth are parallel with one another. Alternatively, we consider systems where Δy_t and Δy_b are unequal, and the saw-tooth walls are not parallel. The choice of $\Delta y_t = 0$, $\Delta y_b \neq 0$ (or vice versa) is a special case of this last group—in this case, the horizontal top wall induces a vertical symmetry such that the dynamics is isomorphic to a system where both top and bottom saw-teeth have height Δy_b, but where the saw-teeth are Δx out of phase, as in the equilibrium mechanical pump of [18]. We will therefore consider these walls as an extension of the first group of parallel saw-tooth walls.

The model described so far can be called an *equilibrium* model, because there is no dissipation of energy. A *nonequilibrium* model can be constructed in the usual way for nonequilibrium molecular dynamics (NEMD) simulations—we introduce an external field ϵ, which accelerates the particle in the positive x direction, and a Gaussian thermostat, which balances the effect of the field by dissipating kinetic energy. For the single particle system, the thermostat acts to keep the speed of the particle a constant of motion. In this case, the particle obeys the equations of motion

$$\left.\begin{array}{ll} \dot{x} = p_x & \dot{p}_x = -\alpha p_x + \epsilon \\ \dot{y} = p_y & \dot{p}_y = -\alpha p_y \end{array}\right\} \quad \alpha = \epsilon p_x \tag{2}$$

until it reaches the boundary $\partial\mathcal{P}$, where it undergoes a specular reflection, as in the equilibrium case. The effect of the field is to curve the trajectories, making them concave in the direction of the field. In fact, the solution of the equations of motion, for the free-flight parts of the trajectory, are given by

[5] A simple mirror symmetry operation allows the equilibrium dynamics of the billiard, defined above, to be reduced to an even simpler fundamental domain than the EC, which is only half of the EC. However, the nonequilibrium dynamics which will be considered later is made of curved trajectories, whose convexity has a precise sign, and is not preserved by the mirror symmetry. Therefore, we do not reduce further the EC.

$$\tan\frac{\vartheta(t)}{2} = \tan\frac{\vartheta_0}{2}\,\mathrm{e}^{-\epsilon t} \tag{3}$$

$$x(t) = x_0 - \frac{1}{\epsilon}\ln\frac{\sin\vartheta(t)}{\sin\vartheta_0} \tag{4}$$

$$y(t) = y_0 - \frac{\vartheta(t) - \vartheta_0}{\epsilon}, \tag{5}$$

which depend on the initial angle ϑ_0. We note that the boundary of this system is not defocusing, and the external field has a focusing effect, so that the overall dynamics should not be chaotic, although it is not obvious that this is the case for all values of ϵ. When the external field ϵ is set to zero, one recovers the usual equilibrium equations of motion.

The data in this paper were obtained from molecular dynamics simulations of the channel transport system described above. In both the equilibrium and nonequilibrium cases, the momentum and position of the particle are determined by solving the free-flight equations of motion. These are solved analytically in the equilibrium case or numerically using a modified regola falsi (MRF) technique in the nonequilibrium case. The tolerance in the time solution for the MRF method was set to 10^{-14} time units—the error is still close to the double precision numerical error of the equilibrium case, while permitting timely convergence. Reported values correspond to averages of distinct simulation runs with different initial conditions for the particle. These initial conditions were randomly generated with a uniform spatial distribution, and a 'circle' velocity distribution, expressed by a probability density

$$\frac{1}{2\pi}\delta(\rho - 1)\,\mathrm{d}\rho\,\mathrm{d}\vartheta, \qquad \text{with velocity } v = \rho(\cos\vartheta, \sin\vartheta) \tag{6}$$

where the speed is $|v| = \rho = 1$.

3. Background theory

Generally, our interest in studying ensemble properties stems from the foundations of statistical mechanics. From a practical viewpoint, when studying a molecular system, we expect that the specific initial microscopic conditions do not alter the thermodynamic properties of a system. That is, we expect an equivalence between the ensemble and time averages of trajectory properties, such that if we were to wait long enough, the average of a property along almost any trajectory would be independent of the initial condition (and equal to the average of the property on the ensemble of initial conditions). Such a phenomenological requirement is incorporated into the theoretical structure of statistical mechanics through the mathematical notion of ergodicity, which can be summarized as follows. Consider a particle system constituted by N classical particles, described by the equations of motion

$$\dot{x} = G(x); \qquad x = (\mathbf{q}, \mathbf{p}) \in \mathcal{M} \subset \mathbb{R}^{6N}, \tag{7}$$

where $\mathcal{M}$ is the phase space, and the vector field G contains the forces acting on the system and the particles' interactions. Denote by $S^t x$, $t \in \mathbb{R}$, the solution of (7) with initial condition x. The macroscopic quantity associated with an *observable*, i.e. with a function of phase $\Phi : \mathcal{M} \to \mathbb{R}$, is defined by

$$\bar{\Phi}(x) = \lim_{T\to\infty}\frac{1}{T}\int_0^T \Phi(S^t x)\,\mathrm{d}t. \tag{8}$$

in which the time average represents the fact that macroscopic observations occur on time scales which are very long compared to the microscopic time scales, so that the measurement

amounts to a long-time average. In general, however, computing that limit is not a trivial task at all. The problem is commonly solved by invoking the EH, which states that

$$\bar{\Phi}(x) = \frac{1}{\mu(\mathcal{M})} \int_{\mathcal{M}} \Phi(y)\, \mathrm{d}\mu(y) = \langle \Phi \rangle_{\mu} \tag{9}$$

for a suitable measure μ (the *physical measure*), and for μ almost all $x \in \mathcal{M}$. In principle, ergodic theory should identify the cases verifying the EH, and the physical measures μ, but in practice, this is too hard, if not impossible, to do. Nevertheless, there is now a vast literature on the validity of the EH, which can be understood in different ways, but which finds in Khinchin's arguments on the properties of sum variables, the most convincing explanation [1]. In practice, the time average of the functions of physical interest in systems of many particles is reached before a trajectory has explored the whole phase space (which would take too long), because such functions are almost constant and equal to the ensemble average. Therefore, the finer details of the microscopic dynamics are not particularly important, except for the requirement of some degree of 'randomness' (in order to introduce a decay in correlations between particles in the system). However, it is not clear what properties should be imposed on the dynamics in order to obtain sufficient randomness. Consequently, in a system devoid of dynamical chaos, such as that under investigation in this paper, it is of interest to investigate the behaviour of both the individual and ensemble properties of particles (and their trajectories).

From a mechanical viewpoint, diffusion can be associated with the motion of tagged particles moving through a host environment of (mechanically) identical particles. From a thermodynamic viewpoint, diffusion is the mass transport process generated by gradients in chemical potential [33, 34]. More commonly, and often more conveniently, this mass transport is described in terms of Fickian diffusion, relating the mass flux to gradients in local density, rather than chemical potential. Through the fluctuation–dissipation relation (which invokes the EH), these nonequilibrium diffusion properties are related to the relaxation of local mass-gradient fluctuations at equilibrium. Therefore, the mass transport in both the equilibrium and nonequilibrium fluids corresponds to the same diffusion transport coefficient, even though the response to an external action and the spontaneous equilibrium fluctuations are rather different phenomena[6]. Fick's first law for diffusion is expressed by [33]

$$\mathbf{J}(\mathbf{x}) = -D\nabla n(\mathbf{x}) \tag{10}$$

where $\mathbf{J}$ is the mass flow, D is the Fickian diffusion coefficient, n is the number density and $\mathbf{x}$ is the position in space. This law, which can be justified in kinetic theory [34], provides the phenomenological basis for the mathematics of diffusion in molecular systems, leading to the second-order PDE

$$\frac{\partial n}{\partial t} = D\frac{\partial^2 n}{\partial x^2}, \tag{11}$$

known as Fick's second law, where t is the time variable. The well-known Gaussian evolution

$$n(x,t) = (4\pi Dt)^{-1/2}\, \mathrm{e}^{-x^2/4Dt} \tag{12}$$

results from an initial delta-function distribution, and the linearity of (11) ensures that the diffusion of a system of molecules can be considered as the evolution of a superposition of Gaussians. In particular, we recover from (12) the linear growth in the mean-square displacement for macroscopic diffusion processes

$$\langle x^2(t) \rangle = \int_{-\infty}^{\infty} x^2 n(x,t)\, \mathrm{d}x = 2Dt. \tag{13}$$

[6] For instance, the spontaneous fluctuations around equilibrium states do not dissipate any energy. Indeed, they do not change the state of the system and continue forever. Differently, the response to an external action dissipates part of the energy received, and may modify the state of the system, or maintain a nonequilibrium steady state.

We note that, if $n(x, t)$ is not a slowly varying function, higher order corrections may be introduced. The next approximation has the form

$$\frac{\partial n}{\partial t} = D\frac{\partial^2 n}{\partial x^2} + B\frac{\partial^4 n}{\partial x^4}, \tag{14}$$

where B is called the *super Burnett* coefficient. In this case, the diffusion coefficient can still be defined as in (13)—furthermore, the super Burnett coefficient can be determined via the relation

$$\langle x^4(t)\rangle - 3\langle x^2(t)\rangle^2 = \int_{-\infty}^{\infty} x^4 n(x,t)\,\mathrm{d}x - 3\left[\int_{-\infty}^{\infty} x^2 n(x,t)\,\mathrm{d}x\right]^2 = 24Bt. \tag{15}$$

As such, the super Burnett coefficient can be seen as a measure of the degree to which transport is diffusive, in the Fickian sense. We note, however, that it has become customary to call *diffusive* any phenomenon displaying a linear relation between the mean-square displacement and time, as in (13). In this paper, we do the same. However, we note the key role played by the assumption of a phenomenological law, such as Fick's, in the preceding argument. In general, for a differing phenomenology, one cannot expect the resulting transport processes to remain diffusive in nature. In the absence of intermolecular interactions (or indeed, of other molecules), there is no phenomenological basis for expecting the mass flux to depend on density gradients, and it is therefore of interest to examine the resulting transport.

In characterizing the transport law, we consider the behaviour of the displacement as a function of the time t, denoted as $s_x(t)$, at equilibrium. In general, we expect an (asymptotic) relation of the form

$$\left\langle s_x^2(t)\right\rangle \sim At^{\gamma} \tag{16}$$

where the coefficient A represents a mobility and the exponent γ indicates the corresponding transport law. The symbol $\langle\cdot\rangle$ indicates an ensemble average, which in equilibrium systems is universally derived from the equal *a priori* probability assumption or the EH. In the following, we adopt the same assumption, when considering equilibrium systems, although it is not obvious that one should necessarily do so. Similarly, we adopt the language of thermodynamics and define the following transport properties:

Definition 3. *Assume that* $\lim_{t\to\infty}\left\langle s_x^2(t)\right\rangle/t^{\gamma} = A$, *for some* $A \in (0, \infty)$, *then* A *is called the mobility coefficient, and*

(i) if the exponent γ *equals 1, the transport is called diffusive;*
(ii) if $\gamma > 1$, *the transport is called super-diffusive and, in particular, it is called ballistic if* $\gamma = 2$ *(the mean-square displacement is proportional to time);*
(iii) the transport is called sub-diffusive if $\gamma < 1$.

Away from equilibrium, it is less straightforward to distinguish between the various transport laws, as the thermostat imposes an upper limit of linear growth for s_x, even for super-diffusive transport processes. In general, for diffusive processes, the diffusion coefficient is determined by the *finite-field, finite-time estimate* of the (nonequilibrium) diffusion coefficient

$$D(\epsilon; t) = \frac{kT\langle v_x(t)\rangle}{m\epsilon} \tag{17}$$

at field ϵ and time t, for a system of particles of mass m at temperature T (with Boltzmann's constant k) and mean streaming velocity of $\langle v_x\rangle$. The existence of a linear regime amounts to the convergence of $D(\epsilon; t)$, in the infinite-time and zero-field limits (at constant T), to a diffusion coefficient D_{ne}:

$$D_{\mathrm{ne}} = \lim_{\epsilon\to 0}\lim_{t\to\infty} D(\epsilon; t) = \frac{kT}{m}\lim_{\epsilon\to 0}\lim_{t\to\infty}\frac{\langle v_x(t)\rangle}{\epsilon} \tag{18}$$

with D_{ne} equal to the equilibrium diffusion coefficient in the same system at zero field.

We define as super-diffusive a nonequilibrium process for which the limit (18) diverges to infinity. We note that, due to the thermostat, the maximum mean value of v_x is equal to the initial speed of the particle v. For initial velocity set to unity, $D(\epsilon; t)$ has an upper bound of $1/2\epsilon$ in our systems, for any ϵ.

4. Results

In this section, we outline the results we have obtained from simulations of the transport of molecules in the saw-tooth channel system described in section 2. We examine the equilibrium transport properties in section 4.1 and the nonequilibrium transport properties in section 4.2. In both cases, we will be interested in the collective, ensemble behaviour of particles in the system, and how this ensemble behaviour relates to the behaviour of individual trajectories.

4.1. Equilibrium

The ergodic properties of our systems are not obvious; therefore, there seems to be no immediate choice for a probability distribution in phase space, to be used for the ensemble averages. Nevertheless, the uniform probability distribution (Lebesgue or Liouville measure, defined above) is invariant, and one could think that it is appropriate for transport in a membrane which receives particles from a reservoir, inside which the dynamics is chaotic. Therefore, the ensemble averages in this section are all computed assigning equal weight to all regions of phase space.

4.1.1. Parallel walls, collective behaviour. In figure 2, we depict the mean-square displacement, as a function of time, for a series of parallel saw-tooth systems ($\Delta y_t = \Delta y_b = \Delta y$). We examine systems where the ratio $\Delta y/\Delta x$ varies from 0.25 to 3, so that the angle $\theta = \theta_t = \theta_b$ the saw-tooth makes with the horizontal varies from about 0.08π rad ($\approx 14^\circ$) to about 0.4π rad ($\approx 72^\circ$). Each graph shows results for a single value of $\Delta y/\Delta x$, for various pore heights h. For each choice of Δy (recalling that $\Delta x = 0.5$), we examined pores with heights $h = 1.5\Delta y, 2\Delta y, 2.05\Delta y, 3\Delta y$ and $21\Delta y$. The corresponding interior pore heights are $d = 0.5\Delta y, \Delta y, 1.05\Delta y, 2\Delta y$ and $20\Delta y$. We note that $h = 2\Delta y$ corresponds to the critical pore width, above which the billiard horizon is infinite (i.e., there is no upper bound to the length of possible molecule trajectory segments without boundary collisions). We considered sets of initial conditions ranging from 1000 to 5000 particles. For clarity, we do not include the error bars on the graphs in this or subsequent figures showing the mean-square displacement as a function of time—however, the error estimates obtained have been used in the determination of the transport law exponents (see below). Not surprisingly, given the clearly non-diffusive nature of the transport observed in figure 2, the corresponding super Burnett coefficients do not appear to have a well-defined value, but diverge over time.

The same data have also been generated for a series of systems with one flat wall and one saw-tooth wall, which always have an infinite horizon. For these systems, we set $\Delta y_t = 0$, and considered the same ratios $\Delta y_b/\Delta x$ as were examined in the parallel saw-tooth systems with pore heights $h = 1.05\Delta y_b, 2.5\Delta y_b$ and $20.5\Delta y_b$ (which have corresponding interior heights $d = 0.55\Delta y, 2\Delta y$ and $20\Delta y$). Sets of initial conditions ranged from 1000 to 5000 particles. There appeared to be a longer initial transient period for the systems with one flat wall, but otherwise the results were qualitatively the same as for the parallel wall, despite the infinite horizon. Table 1 shows the values of the exponents obtained from fitting the data in figure 2 and those for one flat wall to (16), for both the parallel saw-tooth systems and the systems with one flat wall and one parallel wall. Data and error estimates in the table

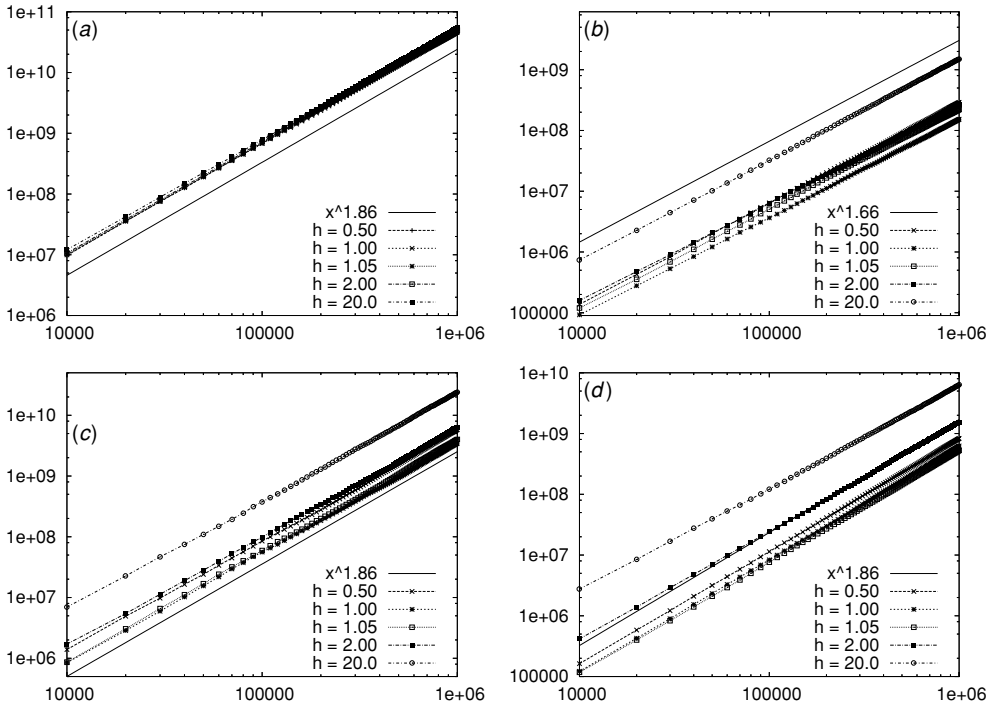

Figure 2. Evolution of mean-squared displacement for parallel saw-tooth systems, for (*a*) $\Delta y/\Delta x = 0.25$, (*b*) $\Delta y/\Delta x = 1$, (*c*) $\Delta y/\Delta x = 2$ and (*d*) $\Delta y/\Delta x = 3$. The data are obtained from 1000 to 5000 initial conditions, and the average number of collisions is of the same order as the total time.

Table 1. Equilibrium transport exponents: for saw-tooth boundary base triangles with height–width ratio $\Delta y/\Delta x$. For each (mean) pore height tested, the observed exponent out to 10^6 time units (of the order of 10^6–10^7 collisions) is given. The number of initial conditions used to compute averages ranges from 1000 to 5000, and the errors are estimated by ± 0.03 in all cases.

	Saw-tooth systems					Saw-tooth/flat systems		
$\Delta y/\Delta x$	$0.5\Delta y$	$1.0\Delta y$	$1.05\Delta y$	$2.0\Delta y$	$20\Delta y$	$0.55\Delta y_t$	$2.0\Delta y_t$	$20\Delta y_t$
0.25	1.85	1.83	1.82	1.85	1.85	1.88	1.83	1.85
1	1.66	1.64	1.62	1.67	1.68	1.65	1.65	1.65
2	1.83	1.85	1.82	1.80	1.79	1.83	1.82	1.75
3	1.86	1.87	1.84	1.80	1.70	1.82	1.76	1.70

were determined using a Marquardt–Levenberg nonlinear least-squares fit of the data and error estimates of individual points. In all cases, we observe that the transport is significantly super-diffusive, but *not* ballistic. For the $\Delta y/\Delta x = 1$ system, which is a (parallel) rational polygonal billiard, we observe an exponent $\gamma \approx 1.65$. All other choices of $\Delta y/\Delta x$ represent (parallel) irrational polygonal billiards. For $\Delta y/\Delta x = 1/4$ (where $\theta < \pi/4$), we observe an exponent of $\gamma \approx 1.85$ in all systems. For $\Delta y/\Delta x = 2$ and $\Delta y/\Delta x = 3$ (where $\theta > \pi/4$), we observe a similar exponent in the systems with pore height less than or in the vicinity of $2\Delta y$ and a *reduction* in the transport exponent as the pore height increases (a corrugation effect). The same value $\gamma \approx 1.85$ has been found by Falcioni and Vulpiani in the equilibrium version of the periodic Ehrenfest gas of [17, 35].

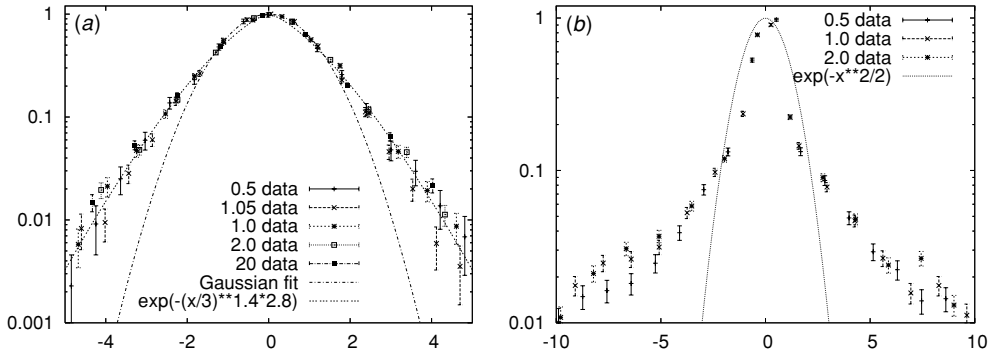

Figure 3. Distribution of displacements after 10^6 time units for parallel saw-tooth systems, where (*a*) $\Delta y/\Delta x = 2$, from 2000 initial conditions and (*b*) $\Delta y/\Delta x = 1$, from 5000 initial conditions.

We have also examined the distribution of the total x displacements $s_x(t)$, as a function of time. Distributions for the $\Delta y/\Delta x = 1$ system (obtained from 2000 initial conditions) and the $\Delta y/\Delta x = 2$ system (obtained from 5000 initial conditions), obtained at the end of the simulations, are shown in figure 3. The results for the $\Delta y/\Delta x = 2$ system are typical of the results observed for the other parallel irrational polygonal billiards. Errors are estimated from the frequency counts used to generate the histograms.

From an initial distribution that is effectively a delta function on the scale of the motion, the transport process produces symmetric distributions, distinct from a Gaussian distribution. For the parallel irrational polygonal billiards, the distribution appears Gaussian out to one standard deviation—however, the distribution at larger displacements is clearly underestimated by the Gaussian. Attempted fits using functions of the form $\exp\{-x^\alpha\}$ fail to capture the shape both at the centre and in the tails, although the tails appear to be well modelled by a distribution of the form $\exp\{-x^{1.4}\}$ (figure 3(*a*)). When $\theta = \pi/4$, however, the distribution bears little resemblance to a Gaussian (figure 3(*b*)). Analogous results in each case were obtained from the systems with one flat wall and one saw-tooth wall.

We have also examined the behaviour of the momenta of particles in our systems. Given that the speed is preserved by the dynamics, the momenta can vary only in orientation, and we therefore examine the effect of the dynamics on the distribution of these orientations. Figure 4 shows the typical behaviour of the distribution of momenta orientations at the beginning, at the midpoint and at the end of a typical simulation of 5000 particles. We also show a mean distribution obtained from averaging the momentum data over all sampled times, as well as over all trajectories. We find that there are no significant correlations in the distributions of the momenta over the course of the simulation. The distribution of orientations does not converge to the uniform distribution over the time scales we have considered (as we might expect for a large system of interacting particles): nor does it appear to diverge further from the uniform distribution. Any memory effects do not appear to have a significant influence on the overall distribution at any instant. Again, the same conclusions can be drawn from similar examination of the systems with one flat wall and one saw-tooth wall.

Remark 1. The dependence of the transport law on the angles θ_i, but not on the pore height, is reminiscent of the behaviour in (chaotically) dispersing billiards. There, the infinite horizon adds a logarithmic correction to the time dependence of mean-square displacement, which is hard to detect numerically. Despite the lack of chaos, our non-dispersing billiards could display similar logarithmic corrections when the horizon is infinite [20].

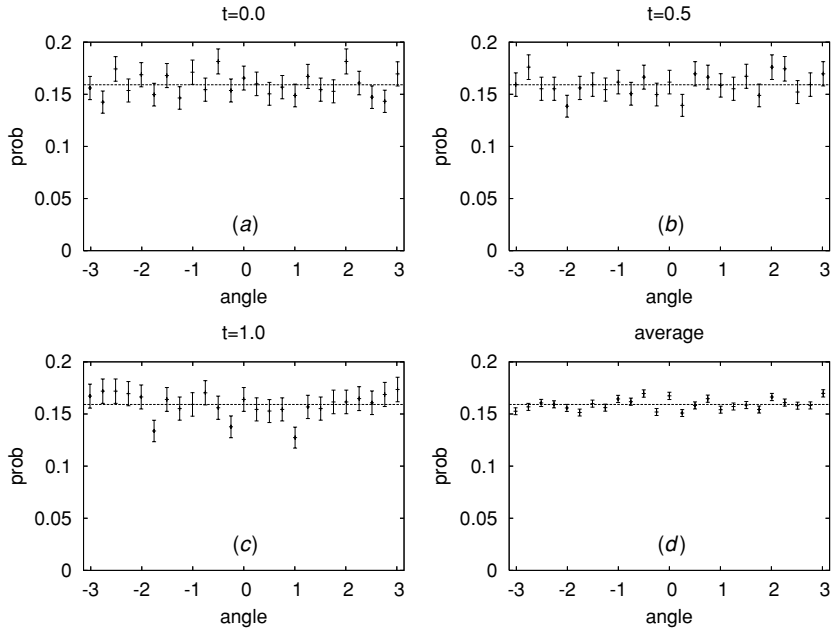

Figure 4. Distribution of momenta orientations at (*a*) $t = 0$, (*b*) $t = 5 \times 10^5$, (*c*) $t = 10^6$ and (*d*) averaged over all times, for the $\Delta y/\Delta x = 1$ system with $d = 0.5\Delta y$. The dotted line indicates the uniform distribution. Errors are estimated from the frequency counts used to generate the histograms (and are hence smaller in (*d*), where the data are comprised of more samples).

More surprising is the observation that in some cases the overall mass transport *decreases* as the pore width increases while the horizon is finite and only increases again once the horizon is infinite.

4.1.2. Parallel walls, individual behaviours. From the results we have obtained, there appear to be well-defined collective behaviours that are attributable to the systems we have studied—that is to say, the mean values of the properties obtained from simulation appear to converge, in the limit of a large number of independent trajectories (or particles), to well-defined values. In analogy to what we have presented above, we examine the evolution of the individual particle momenta and the x displacements.

The picture of the momenta is trivial in the $\Delta y/\Delta x = 1$ systems, because for $\theta = \pi/4$ only four orientations per trajectory at most are possible, as determined by the initial condition. The picture of the momenta for irrational systems appears less predictable. Over the course of the simulations, sequences of momenta, *sampled at intervals of* 10^4 *time units*, were collected. In figure 5, we show such a sequence of momenta, sampled from a system where $\Delta y/\Delta x = 3$, accumulated up to the 5×10^5 time units (figure 5(*a*)), 2×10^6 time units (figure 5(*b*)) and 10^7 time units (figure 5(*c*)). The momenta are represented by symbols (circles) on the unit circle $\boldsymbol{T}^1$, while the lines indicate the sequence of the sampled momenta. It is clear from figure 5 that, despite consisting of up to 1000 different sampled momenta, the number of distinct momenta visited by the particle is relatively small (of the order of 10–20). Furthermore, the growth of this set is gradual, and strongly correlated to the set of momenta that precede it in the sequence of momenta visited by the particle. The choice of θ irrationally related to π permits, in principle, the exploration of the whole unit circle of orientations. However, it is clear that the nature of the sequence of wall collisions limits the rate at which such an exploration of the

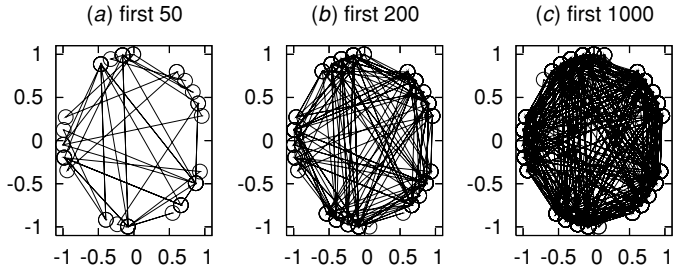

Figure 5. Momentum progression for a single trajectory up to (*a*) $t = 5 \times 10^5$ (50 samples), (*b*) $t = 2 \times 10^6$ (200 samples) and (*c*) $t = 10^7$ (1000 samples), for the $\Delta y/\Delta x = 3$ system with $d = 2\Delta y$.

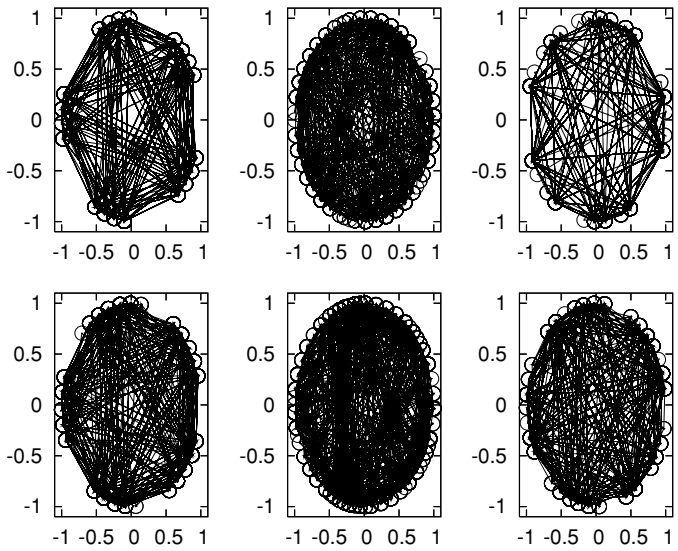

Figure 6. Sequences of sampled momenta for six different initial conditions, up to 10^7 time units (1000 samples), for the $\Delta y/\Delta x = 3$ system with $d = 2\Delta y$.

unit circle can be achieved. This slow growth was observed for simulation times up to 10^9 time units (not shown here).

In figure 6, we show the sequence of the first 1000 momenta, sampled every 10^4 time units, for six distinct initial conditions in a $\Delta y/\Delta x = 3$ system. In each case, the available velocity phase space is gradually explored by the particle. We note that the rate and manner in which this exploration takes place (as indicated by the lines joining consecutive sample momenta) depends significantly, and *unpredictably*, on the initial condition, as is demonstrated by the visibly different structures generated by each. This feature is common to all parallel irrational polygonal billiards examined—for systems with parallel saw-tooth walls and systems with one flat wall and one saw-tooth wall. The flat wall in these latter systems induces a vertical symmetry that is absent in the parallel systems and appears to increase the range of momenta visited by particles—however, a similar degree of connectivity is observed in both cases.

Finally, we turn our attention to the behaviour of the displacements $s_x(t)$ for individual initial conditions, as a function of time, which we expect to give further insight into the manner in which the momentum space is explored. In figure 7, we show $s_x(t)$ as a function of time over four different time scales for a single particle trajectory in a system where $\Delta y/\Delta x = 0.25$.

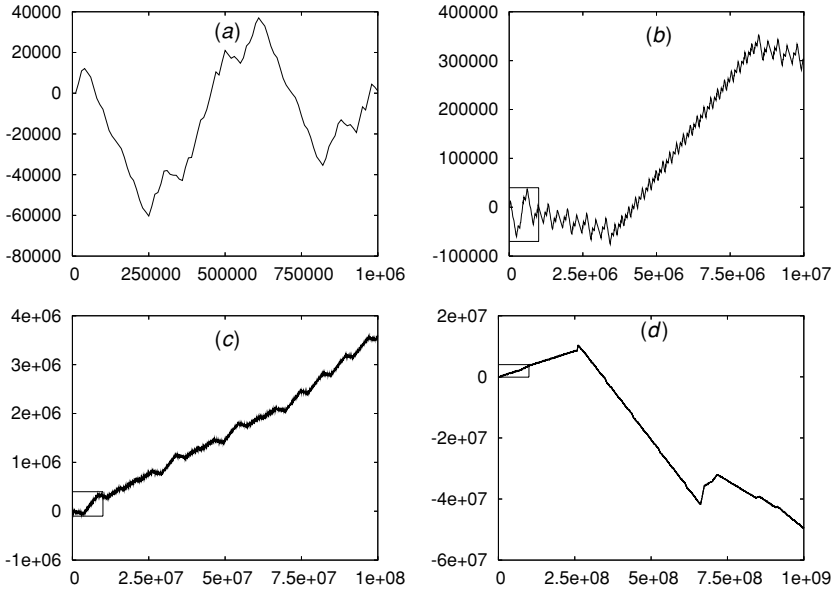

Figure 7. Example of the time evolution of a particle displacement for the $\Delta y/\Delta x = 0.25$ system ($d = 0.5\Delta y$), for a sequence of four different time scales. Boxes indicate the position of the previous graph in the sequence.

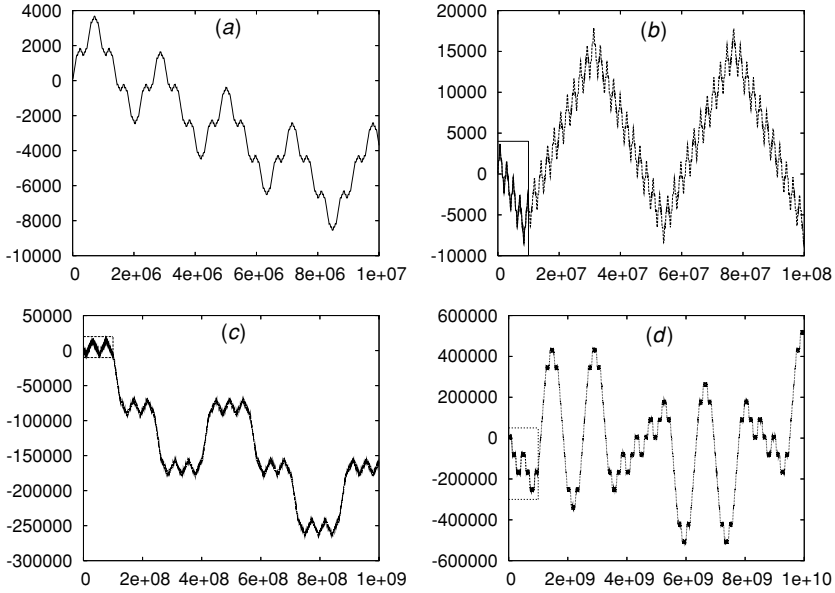

Figure 8. Example of the time evolution of a particle displacement for the $\Delta y/\Delta x = 1$ system ($d = 2\Delta y$), for a sequence of four different time scales. Boxes indicate the position of the previous graph in the sequence.

Again, such a trajectory is typical of the results observed for the parallel irrational polygonal billiards examined. In figure 8, we show an analogous set of results for transport of a particle in a (rational) $\theta = \pi/4$ system.

In figure 7(*a*), the dynamics appear somewhat random on the scale of 10^6 time units, although on closer inspection it is clear that certain sections of the trajectory are repeated. Indeed, the occurrence of repeated segments is more obvious in figure 7(*b*), where after an initial transience of 10^6 steps, the simulation appears to reach a periodic orbit, before changing to another orbit in the interval at about 3.5×10^6, then reverting to the original orbit at around 8×10^6 time units. On a longer time scale (figure 7(*c*)), the transport appears to alternate between these two almost-periodic orbits. However, on the scale of 10^9 time units (figure 7(*d*)), the evolution of s_x takes on quite a different appearance, bearing a similarity with what one might observe for the random motion of a particle in a low-density gas. Such a resemblance suggests that, on this time scale, there could be sufficient memory loss of the preceding momentum values for the trajectory to appear random. Even at this stage, however, the number of distinct momenta visited by the particle is still limited to the order of 10–100.

To give some physical sense to these observations, we consider the analogy of the transport of a light gas (such as methane) along a nanopore of width 1 nm. At room temperature, the unit velocity in our particle corresponds to a root-mean-square velocity for methane of approximately 400 m/s. It follows that our time units correspond to the order of picoseconds. Thus, for the system above, the correlation length is about 10^9 ps = 1 μs, during which the particle will have a net displacement along the pore of the order of millimetres. We note that the mean intermolecular collision time would be much less than this, for all but the most rarefied of conditions.

In contrast, we recall that the transport behaviour in the $\theta = \pi/4$ system is restricted to a maximum of four distinct momenta, for each initial condition. Despite this apparently strong limitation, a richness in behaviour is still evident. In figure 8, we observe strongly recurrent behaviour on all time scales observed, although the nature of the recurrence varies on all observed time scales, and is likely to continue to do so at larger and larger scales. We note that figures 7(*d*) and 8(*c*) represent the evolution of s_x over the same time length—however, while this evolution appears random in the irrational system, the motion is regular in the rational case. The regularity is less trivial in figure 8(*d*), with four small steps between the first two large steps, but only three small steps between the second two large steps, showing that the apparent regularity does not make the dynamics easily predictable. Continuing the physical analogy above, the lower bound for the correlation time in this system is closer to the order of seconds, although the mean displacement over this time is still of the order of millimetres (because of the slower transport, reflected by the smaller value of γ).

In figure 9(*a*), we show the distribution of displacements obtained by dividing the 10^9 time-unit trajectory for the $\Delta y/\Delta x = 0.25$ system into segments of shorter time periods, in order to compare with the approximation to the ensemble distribution obtained from averaging over trajectories with independent initial conditions. It is clear from the figure that the two distributions are significantly different—while the ensemble distribution demonstrates the near-Gaussian properties observed earlier, the distribution from the single trajectory is significantly skewed (as could be expected from figure 7) and has a distribution that is much narrower than that of the ensemble. The correlations observed along the trajectory in figure 7 lead to a distribution of displacements that is not at all characteristic of the ensemble, up to a time of one billion time units.

In figure 9(*b*), we show the distribution of displacements obtained by dividing the 10^{10} time-unit trajectory for the $\Delta y/\Delta x = 1$ system into segments, as done above. In contrast with the results for the $\Delta y/\Delta x = 0.25$ system, the distribution obtained in this fashion shows excellent agreement with the ensemble distribution of trajectories.

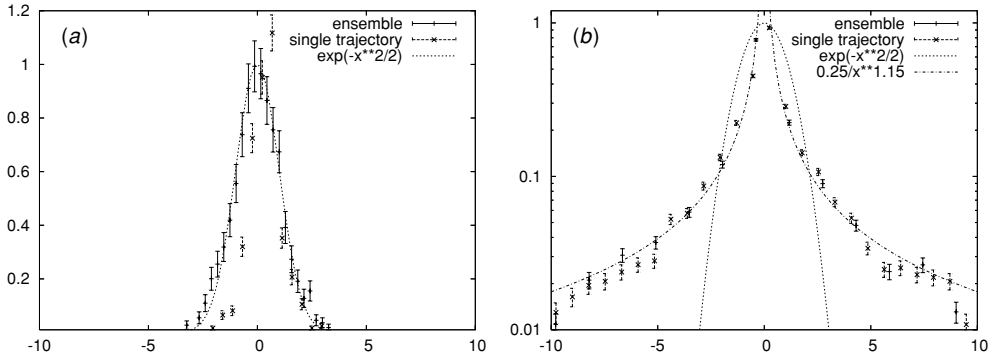

Figure 9. Histogram of displacements collected along a single trajectory, and from the ensemble of trajectories, for the (*a*) $\Delta y/\Delta x = 0.25$ ($d = 0.5\Delta y$) and (*b*) $\Delta y/\Delta x = 1$ ($d = 2.0\Delta y$) systems.

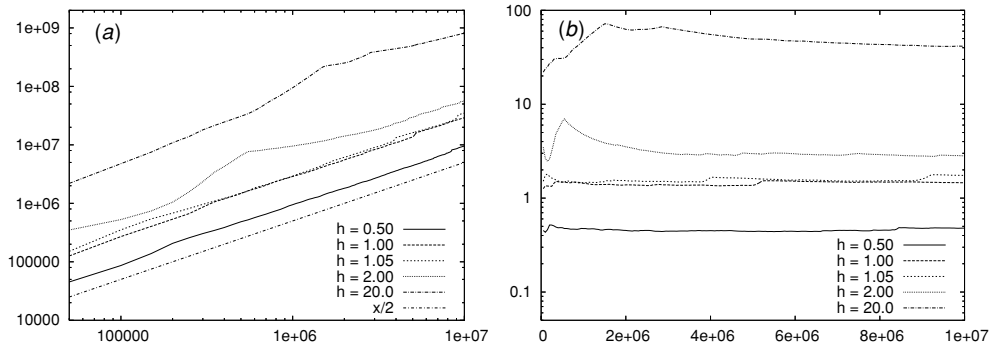

Figure 10. Evolution of (*a*) the mean-squared displacement and (*b*) the diffusion coefficient, for transport in systems with unparallel saw-tooth walls—$\Delta y_t/\Delta x = 0.62$, $\Delta y_b/\Delta x = 0.65$, $d = 0.5d_c, d_c, 1.05d_c, 2d_c$ and $20d_c$.

Remark 2. The overall transport is ultimately *slower* in the rational systems than in the irrational systems. Furthermore, despite the limitations on the velocities that each single trajectory can take, which differ from trajectory to trajectory, the distributions of displacements exhibited by one rational trajectory equal the distribution of the ensemble, while this is not the case for the irrational trajectories!

4.1.3. Unparallel walls, collective behaviours. We have examined the transport properties of a series of unparallel saw-tooth systems, chosen such that the ratios $\Delta y_b/\Delta x$ lie in the vicinity of the golden ratio $(\sqrt{5}+1)/2 \approx 1.618$, so as to 'maximize' the irrationality of the relationship of θ to π. In figure 10, we show the behaviour of the mean-square displacement, and the estimated diffusion coefficient, as a function of time, for a series of unparallel saw-tooth systems where $\Delta x = 0.5$, $\Delta y_t/\Delta x = 0.62$ and $\Delta y_b/\Delta x = 0.65$. In analogy to the results above, we have examined these systems at the same range of pore heights based on the mean interior pore height $d_c = (\Delta y_t + \Delta y_b)/2$ at which the horizon becomes infinite—at $d = 0.5d_c, d_c, 1.05d_c, 2d_c$ and $20d_c$.

Despite containing data from 10 000 independent initial conditions, the data in figure 10 exhibit features suggesting that they have not yet converged to a final result. These features correspond to significant jumps in the mean-squared displacements (and consequently the finite-time estimate of the diffusion coefficient), resulting from short bursts of quasi-periodic

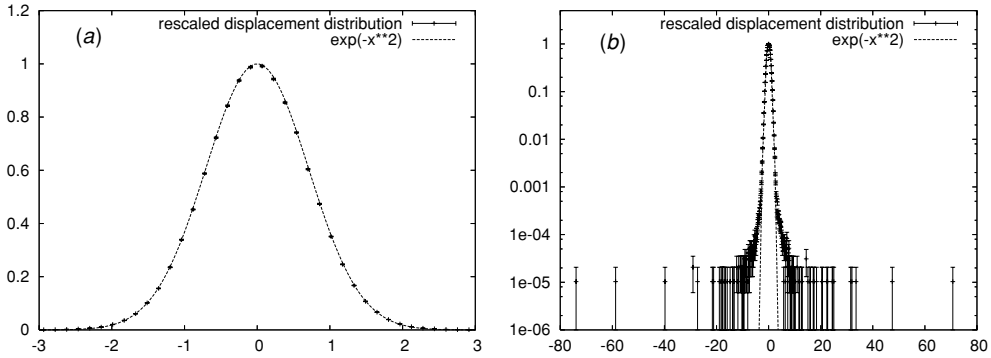

Figure 11. Displacements over intervals of 10^5 time units, combining contributions from all 10^4 initial conditions, for transport in the system $\Delta y_t/\Delta x = 0.62, \Delta y_b/\Delta x = 0.65$, for $d = 0.5d_c, d_c, 1.05d_c, 2d_c$ and $20d_c$: (*a*) within three standard deviations and (*b*) over the full range of displacements (shown using a log-linear plot).

Table 2. Equilibrium transport exponents: for unparallel saw-tooth boundary base triangles with height–width ratio $\Delta y/\Delta x$. For each (mean) pore height tested, the observed exponent out to 10^6 time units (of the order of 10^6–10^7 collisions) is given. The number of initial conditions used to compute averages varies from 2000 up to 10^4. Numbers in parentheses correspond to error estimates from Marquardt–Levenberg least-squares fits.

		Saw-tooth systems				
$\Delta y_t/\Delta x$	$\Delta y_b/\Delta x$	$0.5d_c$	$1.0d_c$	$1.05d_c$	$2.0d_c$	$20d_c$
0.62	0.63	1.00 (2)	1.02 (2)	0.97 (3)	1.03 (7)	0.72 (3)
0.62	0.64	1.00 (1)	1.2 (1)	1.03 (3)	1.19 (7)	1.10 (5)
0.62	0.65	0.99 (2)	1.02 (2)	1.02 (3)	0.97 (6)	1.13 (5)

behaviour (i.e., ballistic transport). We note from figure 10 that the effects of the bursts appear to grow as the horizon is opened. Similar jumps are observed in the time evolution of the super Burnett coefficients, indicating that the bursts contribute to driving the system away from a Gaussian distribution.

To give some sense of the size and frequency of these bursts, we show the distribution of displacements obtained over intervals of 10^5 time units, combining contributions from all 10^4 initial conditions, in figure 11. We observe excellent agreement with the Gaussian distribution, out to several standard deviations. However, in the tail of the distribution we find a non-negligible contribution from large-scale displacements, to which we attribute the behaviour of the super Burnett coefficients. These contributions correspond to the bursts observed in figure 10, and it is clear that a huge number of initial conditions would be required before the overall effect of this tail distribution could be realized by simulation.

Table 2 shows the values of the exponents obtained from fitting the data from the observed systems to (16), and reflects behaviour that is close to diffusive. The significant errors in the data arise from the ballistic bursts, so that a least-squares error estimate, more appropriate for random errors, may not be as appropriate here. However, the least-squares error estimates still provide useful information regarding the relative errors in the data obtained for the various systems.

From figure 11, it is clear that the bursts only occur for a small number of particles. We have found that, in each case, only two or three initial conditions are responsible for the 'significant' bursts—that is to say, if the contribution from these two or three particles

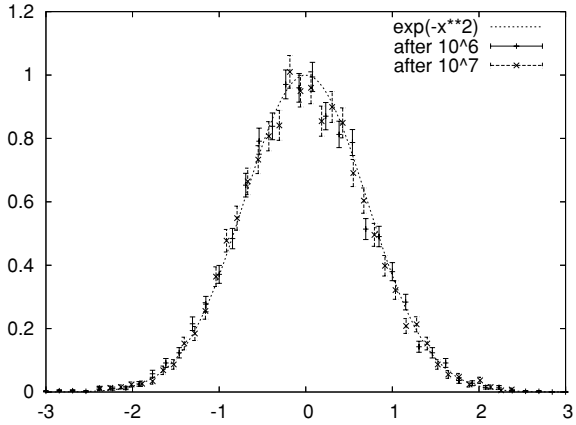

Figure 12. Distribution of final displacements for unparallel saw-tooth systems where $\Delta y_t/\Delta x = 0.62$, $\Delta y_b/\Delta x = 0.65$, $d = 0.5d_c$.

(in 10 000) is neglected, the resultant behaviour is diffusive within statistical error and the fluctuations all lie within error about this mean diffusive behaviour. Within statistical error, one could conjecture that the effect of these 'significant' bursts is not sufficient to drive the behaviour away from diffusive behaviour, given the decay back to diffusive transport observed in figure 10 after each burst. Clearly, however, it cannot be excluded that the effect of these bursts is to drive the transport at a rate somewhat faster than diffusive, either with an exponent slightly greater than 1 or with some slower correction, such as the $\ln t$ correction for the Sinai billiard. This correction has been the subject of recent studies for polygonal channel transport [20]. We note, with the Sinai billiard in mind, that the bursts responsible for this potentially super-diffusive behaviour are observed in systems with both open and closed horizons.

In figure 12, we show the distribution of displacements after 10^6 time units, and after 10^7 time units, from the trajectories of individual particles, again noting that the initial distribution is effectively a delta function since all particles begin from the same unit cell at $s_x = 0$. Even after 10^6 time units, the distribution of displacements is very well fitted by a Gaussian, consistent with our observations of a diffusive transport rate, and in contrast to the results for the parallel walls.

As with the case of parallel walls, the momenta do not appear to be significantly correlated over the course of the simulation, and there is stronger evidence in this case of a convergence to a uniform distribution than in the parallel case.

4.1.4. Unparallel walls, individual behaviours. As with the parallel systems, we have considered the behaviour along longer individual trajectories, to compare with the ensemble behaviour. For unparallel walls, we find that there is strong agreement between the individual and ensemble behaviours, in terms of the distribution of both the momentum orientations and of the displacements. Sequences of momenta appear random along a trajectory, and the distribution of displacements obtained along a single trajectory demonstrates an excellent Gaussian fit, in agreement with the ensemble results.

4.2. Nonequilibrium

An alternative method of studying the transport behaviour is to consider the dynamics in the presence of an external field. For thermodynamic fluids, we expect that the transport coefficient

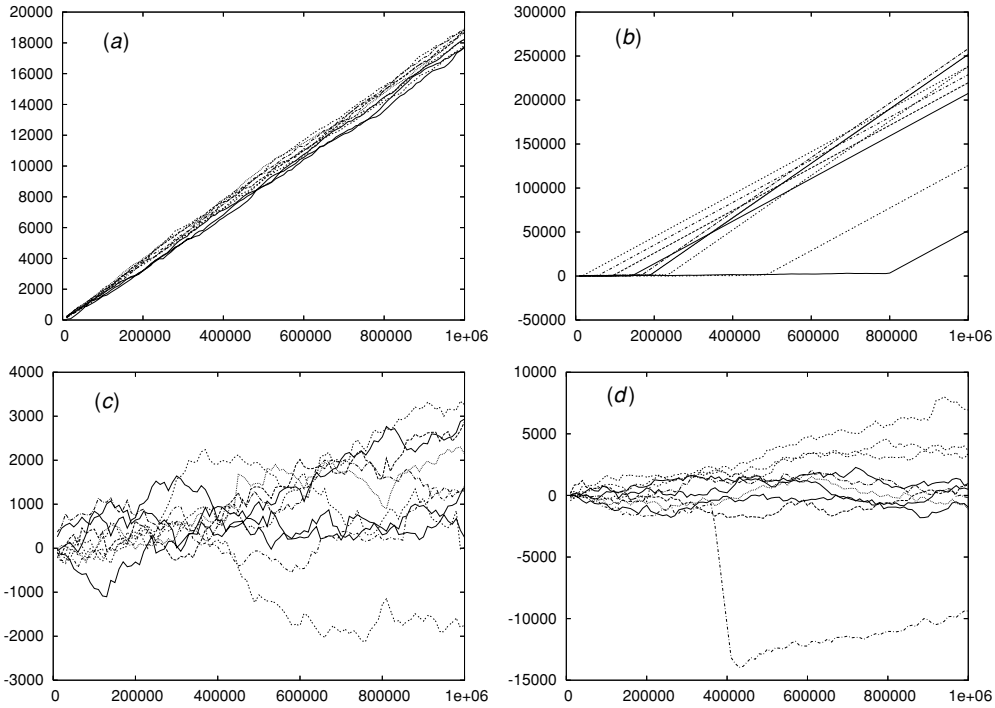

Figure 13. Displacement versus time for ten trajectories for the parallel $\Delta y/\Delta x = 2$ system, for (*a*) $\epsilon = 0.1$, (*b*) $\epsilon = 0.01$, (*c*) $\epsilon = 10^{-3}$ and (*d*) $\epsilon = 10^{-4}$.

determined in the linear response regime (i.e., in the zero-field limit) for the nonequilibrium fluid corresponds to that obtained from the equilibrium fluid properties. It is not clear, *a priori*, that such an equivalence holds for the system examined in this paper, so we examine the nonequilibrium transport properties, as a dynamical system of interest in its own right, as well as to compare its behaviour with that of the equilibrium counterpart.

4.2.1. Parallel. For the non-zero-field estimates of the transport coefficient for the $\Delta y = 2$ system, with $d = 0.5\Delta y$, for the four different field strengths $\epsilon = 0.1, 0.01, 10^{-3}$ and 10^{-4}, we find that the qualitative behaviour of the particles is highly, and unpredictably, dependent on the field strength. At the highest field, $\epsilon = 0.1$ (figure 13(*a*)), all trajectories have similar qualitative and quantitative properties, demonstrating a 'fluid-like' response to the external field—particles are driven in the direction of the field, and the fluctuations about a mean transport rate are small, since the field is strong. At $\epsilon = 0.01$, however, the trajectories exhibit two distinct transport phases—an initial phase where the particle trajectories fluctuate about a mean motion due to the driving field and a second ballistic phase, where the trajectory finds a periodic orbit (figure 13(*b*)). At this field, two distinct orbits were noted—one consisting of 33 reflections, with period $\tau = 9.695\,0889\ldots$ and mean net speed $v_b \approx 0.31$, the other consisting of 39 reflections, with period $\tau = 12.393\,386\ldots$ and mean net speed of $v_b \approx 0.24$. The orbits are shown in figure 14. In particular, we note the existence of distinct periodic orbits to which the different trajectories converge, demonstrating that the dynamics at this field strength is *not ergodic*. At lower fields, a transition to periodic orbits is much rarer—however, bursts of almost-periodic orbits are observed, which decay after relatively short times to revert to the previous apparently random behaviour (figure 13(*d*)).

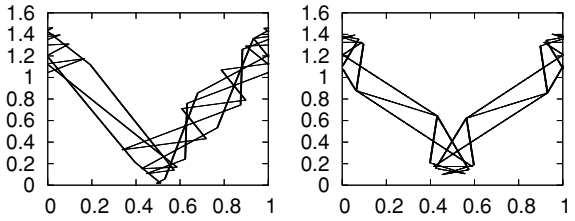

Figure 14. Two distinct periodic trajectories of the finite-field transport for the parallel $\Delta y/\Delta x = 2$ system for $\epsilon = 0.01$. The left-hand side orbit has period $\tau = 12.393\,386\ldots$ time units with 39 reflections per orbit. The right-hand side orbit has period $\tau = 9.695\,0889\ldots$ time units with 33 reflections per orbit.

Table 3. Best estimates of the finite-field diffusion coefficient $D(\epsilon; t)$ for $0.1 < \epsilon < 10^{-4}$, $t = 10^6$ for the parallel $\Delta y/\Delta x = 2$ system, and the unparallel $\Delta y_t/\Delta x = 0.62$, $\Delta y_b/\Delta x = 0.65$, $d = d_c$ system, showing the raw data and data corrected for periodic orbits. Also included, for comparison, are the equilibrium results for the parallel case (exhibiting super-diffusive behaviour) and the unparallel case.

Field strength ϵ	Parallel system (raw)	Parallel system (corrected)	Unparallel system (raw)	Unparallel system (corrected)
0.1	0.0935 ± 0.0001	0.0935 ± 0.0001	2.390 ± 0.003	2.390 ± 0.003
0.01	9.75 ± 0.2	0.205 ± 0.008	18.3 ± 0.2	0.24 ± 0.04
0.001	0.57 ± 0.04	0.57 ± 0.04	11 ± 1	0.19 ± 0.02
0.0001	0.28 ± 0.4	0.28 ± 0.4	1.2 ± 1	0.28 ± 0.14
Equilibrium	∞	∞	0.386 ± 0.05	0.386 ± 0.05

This transition from apparently random transport to ballistic transport has been observed previously in a similar nonequilibrium system with straight walls [17]. There, a transition time was observed between these two transport behaviours, which varied as the inverse square of the external field strength. Our results appear to be consistent with such a relationship, inasmuch as the fraction of observed periodic orbits (indicating ballistic transport) decreases as the field strength increases. We expect that longer simulations would produce a larger fraction of such periodic orbits and suggest that the reason we do not observe any ballistic transport in the weakest field is due to the much larger time scale on which such a transition would take place. Unlike the systems in [17], where only the ensemble behaviour was studied, and a smooth transition from diffusive to ballistic transport was observed at finite times, here we consider the single trajectories and find that their individual transitions are sharp and occur apparently at times not limited by any upper bound.

We show the estimates of $D(\epsilon; t)$ for the applied fields ϵ for the parallel $\Delta y/\Delta x = 2$ system in column 2 of table 3. Over such a range of fields, we would expect to observe either convergence to a well-defined value (the diffusion coefficient) or divergent behaviour (bounded by the thermostat). However, we note that $D(\epsilon; t)$ does not diverge in the zero-field limit, as we would expect for a real fluid which exhibited super-diffusive equilibrium behaviour (such as plug flow).

4.2.2. Non-parallel. In contrast to the results for the parallel systems, we find that the individual particle trajectories for the $\Delta y_t/\Delta x = 0.62, \Delta y_b/\Delta x = 0.65, d = 0.5d_c$ system display the same characteristic behaviour for the four different field strengths $\epsilon = 0.1, 0.01, 10^{-3}$ and 10^{-4} examined. Trajectories are typified by an initial apparently

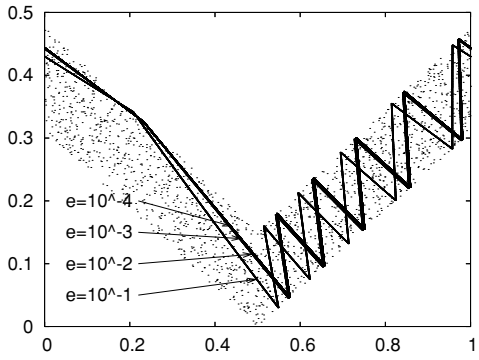

Figure 15. (Attractive) periodic trajectories of the finite-field transport for the $\Delta y_t/\Delta x = 0.62, \Delta y_b/\Delta x = 0.65, d = d_c$ system, for $0.1 < \epsilon < 10^{-4}$. The trajectories for the two weakest fields are indistinguishable on the scale of the figure. Cloud shown for aesthetic reasons.

random transient behaviour, followed by a transition to ballistic transport in a periodic orbit. The transition time also appears to vary inversely with the field strength. As a consequence, the fraction of trajectories observed to undergo a transition within 10^6 time units decreases with decreasing field, and therefore the lifetime of the non-ballistic regime grows.

These results are consistent with those of [17], which were obtained using *parallel* boundary walls, where the wall angles were chosen such that $\tan\theta$ was close to the golden ratio. It is possible that such a choice leads to much smaller correlation times in the momentum sequence for particle trajectories, and consequently faster convergence to the longer time-scale behaviour more reminiscent of intermolecular collisions, observed in figure 7.

For a given field strength ϵ, each ballistic trajectory appears to have the same mean net speed. For each field strength considered, this mean net speed appears to be $v_b \approx 0.48$. We find that the individual trajectories converge to a single periodic orbit that is independent of the initial conditions, but dependent on the field strength. These orbits are shown in figure 15. We note that these periodic orbits appear to be instances of a continuous family of periodic orbits, converging to a limiting orbit in the zero-field limit. However, this limiting orbit is never observed in the equilibrium trajectories, where it is no longer an attractor.

The existence of a family of attractive periodic orbits, converging to a precise periodic orbit in the zero-field limit, precludes the existence of a linear regime, and is significantly at odds with what one would expect of an ergodic, diffusive system in nonequilibrium. For such systems, we would anticipate the convergence of the nonequilibrium finite-field estimates $D(\epsilon; t)$ to the equilibrium value D in the zero-field, infinite-time limit. However, the limiting periodic orbit with a finite net speed $v_b \approx 0.48$ implies that the finite-field, finite-time estimate $D(\epsilon; t)$ must *diverge* as the field goes to zero.

However, as noted above, the fraction of trajectories that turn ballistic within a given time t decreases with decreasing field, so that in the $\epsilon \to 0$ limit we expect this fraction to tend to 0. Furthermore, the behaviour of the trajectories *before* they reach a periodic orbit remains apparently random and responsive to the field. Consequently, we consider the following approach to constructing a 'weak' linear regime. At any given time, we neglect those trajectories already captured by a periodic orbit (i.e., whose transport has become ballistic) and we define a finite diffusion coefficient based upon the remaining trajectories. Usually, one defines the nonequilibrium diffusion coefficient (following the Green–Kubo result (18)) by taking the limits $t \to 0$ and $\epsilon \to 0$ separately—here, this is no longer possible if we wish to avoid periodic trajectories, so the limits must be taken simultaneously.

Therefore, given a sufficiently large ensemble of N particles, assume that the fraction $\nu(\epsilon; t)$ of particles which are still in the diffusive regime, at time t and for field strength ϵ, is well defined. Let $M(N; \epsilon; t)$ be the subset of indices in $\{1, \ldots, N\}$ of these still-diffusive trajectories. Assume that for every $\delta > 0$ there is a field $\epsilon_\delta > 0$ such that $\nu(\epsilon; t) \geqslant 1 - \delta$ if $\epsilon < \epsilon_\delta$ and N is sufficiently large, as seems to be the case in our simulations. For simplicity, assume that there is a function $\epsilon = \epsilon(t; \delta)$, such that $\nu(\epsilon(t; \delta); t) = 1 - \delta/2$. Finally, define $N(\delta) = [2l/\delta]$, where $[\cdot]$ represents the integer part, and choose integer l so large that $N(\delta)$ is sufficiently large for the fraction $\delta/2$ to be sufficiently finely realized, for any $\delta > 0$.

Definition 4. *For every $\delta > 0$, distribute at random (with respect to the Lebesgue measure) $N(\delta)$ initial conditions in the phase space. For each of them and for fixed t, consider*

$$D_i^*(\epsilon; t) = \frac{kT v_{i,x(t)}}{m\epsilon}, \qquad i \in \{1, \ldots, N\},$$

where $v_{i,x}(t)$ is the mean x-component of the velocity of the ith trajectory at time t (and other variables defined as in (17)). The weak nonequilibrium estimate of the diffusion coefficient, if it exists, is defined by

$$\begin{aligned} D_{ne}^* &= \lim_{\delta \to 0} \lim_{t \to \infty} \frac{1}{N(\delta)\nu(\epsilon(t; \delta); t)} \sum_{i \in M(N(\delta); \epsilon; t)} D_i^*(\epsilon(t; \delta); t) \\ &= \lim_{\delta \to 0} \lim_{t \to \infty} \frac{kT}{m\epsilon(t; \delta)} \frac{1}{N(\delta)\nu(\epsilon(t; \delta); t)} \frac{1}{t} \sum_{i \in M(N(\delta); \epsilon; t)} s_{xi}(t). \end{aligned} \tag{19}$$

Thus, for a given choice of δ, and t, we evaluate the estimate of the diffusion coefficient (17) considering only those trajectories which have not been captured by a periodic orbit. Then, the limit $t \to \infty$ includes also the limit $\epsilon \to 0$, and the limit $\delta \to 0$ includes the limit $N \to \infty$. We can now define the following:

Definition 5. *If the equilibrium system has a finite diffusion coefficient D, and $D_{ne}^* = D$, the system is said to have a weak linear regime.*

In table 3, we report the 'corrected' estimates $D^*(\epsilon; t)$ for the various fields, where we neglect contributions from ballistic trajectories. In the third column, we report estimates for the parallel $\Delta y/\Delta x = 2$ system, and in the fifth column we report estimates for the unparallel $\Delta y_t/\Delta x = 0.62$, $\Delta y_b/\Delta x = 0.65$, $d = 0.5 d_c$ system. We note that the 'corrected' data for the parallel $\Delta y/\Delta x = 2$ system are consistent with a divergent trend (taking into account the large statistical error in the weakest field). For the unparallel system, the equilibrium and nonequilibrium transport properties become more consistent, although they are not conclusively so, because of the large error bars produced by the statistical analysis at low field. Such noise is typical of NEMD simulations at low field, where the signal-to-noise ratio becomes low. Typical NEMD simulations, however, would still converge to yield the same transport coefficient in the long-time limit—in our non-chaotic systems, the transition from random to ballistic behaviour effectively places an upper bound on the time during which random behaviour can be observed. The estimated errors in the diffusion coefficient obtained will therefore depend on the rate at which the mean transition time increases with decreasing field.

Remark 3. This subsection leads us to conclude that the use of thermostats needs some form of chaos, whether permanent or transient, in order for a linear regime to be observed. This is a cause for concern in the case of thermostated *non-interacting* particle systems.

5. Transport complexity

As we have seen, the transport properties of the dynamics in these systems we have studied are strongly dependent on the angles θ_i. Dependence of thermodynamic properties on the boundary geometry is a well-studied phenomenon in models of porous media or systems which resemble them. For certain chaotic dynamical systems of non-interacting particles, these thermodynamic properties are known to vary irregularly as a function of boundary parameters [23–27]. However, all of these systems exhibit diffusive transport, irrespective of the variation of the diffusion coefficient. By contrast, the transport processes of the non-chaotic systems in this paper demonstrate an unpredictability of the exponent γ determining the transport *law*, as well as of the corresponding mobility coefficient.

It would therefore seem that the non-chaotic transport studied in this paper is, in some sense, more unpredictable than transport in their chaotic counterparts, and thus more complex [36]. This conceptual connection between unpredictability and complexity can be understood through the perspective of information theory. The unpredictability of a system is related to the information required to describe the system state—less predictable systems require more information to describe them and can therefore be interpreted as more complex. Studies of the complexity of polygonal billiards already appear in the literature, based on the symbolic dynamics of particle trajectories. In such studies, the growth of the number of permitted 'symbolic trajectories' with trajectory length gives a measure of the complexity of the system.

In chaotic systems, nearby trajectories separate at an exponential rate in phase space, and the symbolic dynamics of such systems admits a range of 'symbolic trajectories' that grows exponentially with the trajectory length. However, while non-chaotic systems can also exhibit a sensitivity to initial conditions, nearby trajectories do not separate at an exponential rate in phase space, and the number of allowed 'symbolic trajectories' grows sub-exponentially [21]. From this microscopic measure of complexity, one would conclude that the chaotic systems are more complex than the non-chaotic systems—a conclusion that seems in complete contradiction to the observed macroscopic behaviour.

It is precisely at this distinction between microscopic and macroscopic behaviour that the apparent contradiction arises. The mixing properties of chaotic dynamics causes almost all trajectories to have the same macroscopic properties. If there are super-diffusive or sub-diffusive trajectories permitted over finite symbolic trajectories, the proportion of such trajectories, compared with all allowed trajectories, must go to zero in the infinite-time limit. If all but a negligible set of trajectories are diffusive in this limit, then the only possible variation (and hence unpredictability) in the transport process must be at the level of the mobility coefficient. In the non-chaotic case, diffusive trajectories do not always dominate the set of allowed trajectories in the large time limit, and the unpredictability of the transport processes extends to the exponent γ as well as to the mobility coefficient. We believe that it is of great significance to note that the measure of complexity at the microscopic level *does not reflect* the unpredictability of the transport properties we are interested in at the macroscopic level.

Other non-chaotic maps have been observed to demonstrate a similar class of complexity as those in this paper—see [37] (where the geometry unpredictably gave periodic, diffusive or ballistic behaviour) and [38]. Our numerical results indicate that the transport law can change from diffusive to sub-diffusive regimes or alternatively quite high super-diffusive regimes, after small changes of the parameters defining the geometry. To quantify this kind of complexity, we propose the following definitions.

Definition 6. *Consider a transport model, whose geometry is determined by the parameter* y*, which ranges in the interval* $[0, h]$ *and such that its transport law is given by*

$$\lim_{t\to\infty} \frac{\langle s_x^2(t)\rangle}{t^\gamma} = A, \qquad 0 < A < \infty \tag{20}$$

with γ a function of y varying in $[0, 2]$, when y spans $[0, h]$. Let $\Delta\gamma(y_m, y_M) \in [0, \infty]$ be the difference between the largest and the smallest value of γ, for y in the subinterval $(y_m, y_M) \subset [0, h]$, where $\Delta\gamma(y_m, y_M) = \infty$ if in (y_m, y_M) there are points for which (20) is not satisfied by any $\gamma \geqslant 0$.

(i) The transport complexity of first kind of the transport model in (y_m, y_M) is the number

$$\mathcal{C}_1(y_m, y_M) = \frac{h\Delta\gamma(y_m, y_M)}{2(y_M - y_m)} \in [0, \infty) \tag{21}$$

if it exists.

(ii) The transport complexity of second kind of the transport model for $y = \hat{y}$ is the exponent $\mathcal{C}_2 = \mathcal{C}_2(\hat{y})$, if it exists, for which the limit

$$\lim_{\varepsilon\to 0} \frac{\mathcal{C}_1(\hat{y} - \varepsilon, \hat{y} + \varepsilon)}{\varepsilon^{\mathcal{C}_2(\hat{y})}} \tag{22}$$

is finite.

(iii) The transport complexity of third kind of the transport model for $y = \hat{y}$ is the limit

$$\mathcal{C}_3(\hat{y}) = \lim_{\varepsilon\to 0} \Delta\gamma(\hat{y} - \varepsilon, \hat{y} + \varepsilon). \tag{23}$$

These definitions are motivated by the following considerations. If $\mathcal{C}_1$ does not vanish, the system is surely highly unpredictable from the point of view of transport, in the interval (y_m, y_M), because its transport law is only known with a given uncertainty. This could be the case, for instance, of a batch of microporous membranes with flat pore walls, whose orientation is obtained with a certain tolerance (transport complexity of first kind). However, $\mathcal{C}_1$ may diverge around some point of $[0, h]$, as our data seem to indicate, giving rise to an even higher level of transport complexity. Assuming that this divergence has the form of a power law, we take the power as a measure of this second kind of complexity. But even this level of complexity seems to be insufficient for our models, which indicate that $\Delta\gamma(y_m, y_M)$ could be discontinuous. For this reason, we introduce the third kind of transport complexity.

In order to further investigate these notions, and how they relate to our systems, we have considered the transport behaviour in a narrow range about two principal systems, taken from the examples of super-diffusive transport observed in section 4.1. The first principal system is the rational parallel $\Delta y_t/\Delta x = 1$, where we consider the transport behaviour in the limit that $\Delta y_b/\Delta x \to 1, \Delta y_b/\Delta x > 1$. The second principal system is the irrational parallel $\Delta y_t/\Delta x = 2$ system, where we consider the transport behaviour in the limit that $\Delta y_b/\Delta x \to 2, \Delta y_b/\Delta x > 2$. In table 4, we show the exponent γ of the transport laws (as per (20)) corresponding to the various choices for Δy_t and Δy_b.

We note that, in both cases, there appears to be a strong discontinuity at $\Delta y_t = \Delta y_b$—when the walls are not parallel, the behaviour is no longer super-diffusive. In the rational case, the transport coefficient appears to depend unpredictably on Δy_t, but is always distinctly *sub-diffusive*. By contrast, in the irrational case, the transport appears to be essentially diffusive when the walls are not parallel. This behaviour is consistent with that observed in section 4.1.3 for the unparallel walls, which are also irrational.

Due to the discontinuity, the transport complexities $\mathcal{C}_1$ and $\mathcal{C}_2$ diverge in these cases, reflecting the high degree of unpredictability that has been observed in the previous sections, which can only be quantified by $\mathcal{C}_3$.

Table 4. Transport law exponent, γ, as identified by (20), observed for various choices of $\Delta y_t/\Delta x$ and $\Delta y_b/\Delta x$. There appears to be no trend towards super-diffusive transport, arbitrarily close to (but away from) the parallel case. Numbers in parentheses indicate errors in the last figure.

$\Delta y_t/\Delta x$	$\Delta y_b/\Delta x$	γ	$\Delta y_t/\Delta x$	$\Delta y_b/\Delta x$	γ
1	1.01	0.71 (4)	2	2.02	1.04 (2)
1	1.001	0.35 (6)	2	2.002	1.01 (2)
1	1.0001	0.66 (5)	2	2.0002	1.04 (2)
1	1.000 01	0.58 (3)	2	2.000 02	1.02 (2)
1	1.000 001	0.53 (5)	2	2.000 002	0.98 (2)
1	1	1.66 (3)	2	2	1.83 (3)

6. Conclusion

In this paper, we have examined the transport properties of a dynamical system of remarkable simplicity—a two-dimensional channel with straight-edged walls, populated by non-interacting, point-like particles. In spite of the absence of dynamical chaos, this system displays a rich variety of transport behaviours.

In the equilibrium systems, we observe sub-diffusive, diffusive and super-diffusive transport (although no ballistic behaviour). This behaviour is strongly dependent on the angles θ_i and only weakly dependent on the pore height. The opening of the horizon appears to encourage super-diffusive 'bursts' in the diffusive systems, possibly inducing a time-dependent divergence of the diffusion coefficient. In the super-diffusive systems, opening the horizon appears to *reduce* the exponent γ, although the overall mass transport is greater. This result suggests that wall reflections lead to greater randomness in wider pores, where the dynamics resembles transport along a corrugated channel, and that the sequence of wall collisions is less restricted than in the narrower pores, leading to slower, more diffusive transport. Also in the parallel systems, we note the curious phenomenon whereby the transport coefficient appears to increase as the pore width is decreased, once the horizon has been closed.

The difference in behaviour of trajectories in the diffusive and super-diffusive systems is clear, in terms of the correlation of successive momenta. In the diffusive systems these correlations die off quickly, whereas they produce quasi-periodic 'building blocks' in the super-diffusive trajectories, observable on various length scales. Despite these correlations, the trajectory behaviour is seemingly unpredictable from one order of magnitude of time to the next. While parallel systems with irrational θ can in principle access the whole momentum space, it is only on the scale of some 10^{10} time units that apparently random behaviour is observed. This raises the interesting possibility that the behaviour could indeed become diffusive on longer trajectories, but only on such (computationally expensive) time scales. There is no evidence on the time scales studied of such a possibility for the rational system, which is a reflection of the finite number of distinct momenta accessible along a single trajectory in such systems.

In no case have we observed nonequilibrium transport behaviour that appears to correspond to the associated equilibrium system. In the case of super-diffusive behaviour at equilibrium, one would expect the finite-field diffusion coefficients to diverge in the limit of zero field. Such a divergence would have an upper bound inversely proportional to the field strength. For the systems which are diffusive at equilibrium, we would expect the finite-field estimates to converge to the equilibrium diffusion coefficient. Instead, we find that the finite-field estimates do not clearly diverge for the systems that are super-diffusive at equilibrium and that they clearly *do* diverge for systems that are diffusive at equilibrium, due to the existence of attractive periodic orbits.

For the nonequilibrium parallel systems, the existence of and convergence towards periodic orbits appears irregularly determined by the field strength. We observe clearly non-ergodic behaviour for one field strength, with the existence of distinct attractive periodic trajectories for a single dynamical system. For the nonequilibrium unparallel systems, there is a much more regular field dependence of the transport behaviour. Each trajectory converges towards a periodic orbit which is unique for a given field (and appears to be continuously dependent on the field), and the mean onset time of the periodic orbit grows with decreasing field strength.

Importantly, we note that the absence of clear 'thermodynamic' behaviour tends to support the existing CH, such as those in [3]. Interestingly, however, there appears to be the possibility of a weak linear regime, *before* the onset of the periodic behaviour in the unparallel systems. This approach requires the alternative definition of a 'weak' linear regime, using a non-standard order of the time and field-strength limits. Our results on the existence of this 'weak' linear regime and its thermodynamic interpretation are unclear and are a source of ongoing research.

The range of transport behaviours we have observed, and their unpredictability, raise an interesting contradiction with regards to existing methods for quantifying the complexity of a system. These existing methods focus on the application of information theory at the microscopic level, to determine the unpredictability, and thus the complexity, of the microscopic behaviour. Such an approach would suggest that chaotic systems should be more complex than unchaotic systems—an interpretation that seems intuitively at odds with the behaviour of macroscopic properties such as the overall transport. The reason for this contradiction lies in the fact that, while the chaotic system can exhibit a greater 'diversity' of trajectories than the non-chaotic systems at the microscopic level, they correspond to a smaller 'diversity' of overall transport behaviours. It is this diversity with respect to a particular macroscopic property of interest that we aim to incorporate in our quantification of transport complexity. More complicated notions of transport complexity may then be envisaged, but the conceptual picture outlined here would not change. We note that there may be some degree of subjectivity to our definition of transport complexity, to the extent that we consider 'diversity' with respect to a particular property. This aspect of our notions is one avenue of further investigation.

We note that, for the sake of simplicity, we have focused on the dependence of the transport law on just one parameter, but our investigation reveals that transport in our models may depend in a counterintuitive and irregular fashion on other parameters as well, such as pore height. We anticipate that these notions will be useful in distinguishing between various transport systems, with reference to the diversity of transport properties that they exhibit, and in particular the predictability of these transport properties. For example, slight differences in the manufacturing of porous membranes may result in totally different transport properties.

This analysis leads us to the following observation. As is well known, the thermodynamical properties of a macroscopic system are not a function of the system boundary; the nature of transport and the transport properties of a fluid are essentially independent of the geometry of its container. Fermi expressed this concept, at the beginning of his book on thermodynamics [39]: '*The geometry of our system is obviously characterized not only by its volume, but also its shape. However, most thermodynamical properties are largely independent of the shape, and, therefore, the volume is the only geometrical datum that is ordinarily given. It is only in the cases for which the ratio of surface to volume is very large (for example, a finely grained substance) that the surface must be considered*'. This is clearly understood in the terms of kinetic theory, which leads to explicit expressions for the diffusion coefficients in terms of only the mean-free paths λ for collisions among particles, without any reference to the shape of the container. Only in the case that λ is of

the same order as the characteristic lengths of the container, does this play a role; but in that case, the standard laws of thermodynamics cease to hold and are replaced by those of highly rarefied gases or Knudsen gases [33, 40, 41]. Since our results do not display significant dependence on the surface–volume ratio, they indicate that our systems cannot be considered as thermodynamic systems, much as they remain highly interesting and important from both theoretical and technological standpoints. Indeed, as has been noted elsewhere [42, 43], much care must be taken in the thermodynamic interpretation of the collective behaviour of systems of non-interacting particles. The arguments of [42, 43] mainly referred to nonequilibrium systems: here we provide some examples which show that they apply to equilibrium systems as well. All this can be summarized stating that a certain degree of *chaos* or of *randomness* is required in the microscopic dynamics of particle systems, for them to look like thermodynamic systems, but there are two ways in which this can be achieved. If the randomness is intrinsic to the fluid, the geometry of the system is a secondary issue, and the fluid behaves as a proper thermodynamic system. If the randomness is produced by the geometry of the outer environment, the geometry plays an obviously important role, and systems such as ours do not behave like proper thermodynamic systems.

Acknowledgments

We would like to thank R Artuso, F Cecconi, M Falcioni, R Klages, A Lesne and A Vulpiani for helpful feedback from preliminary drafts. We would also like to thank the ISI Foundation for financial support throughout this work.

References

[1] Khinchin A I 1949 *Mathematical Foundations of Statistical Mechanics* (New York: Dover)
[2] Gallavotti G 1999 *Statistical Mechanics: A Short Treatise* (Berlin: Springer)
[3] Gallavotti G and Cohen E G D 1995 Dynamical ensembles in stationary states *J. Stat. Phys.* **80** 931
[4] Gaspard P 1998 *Chaos, Scattering and Statistical Mechanics* (Cambridge: Cambridge University Press)
[5] Evans D J, Searles D J and Rondoni L 2005 Application of the Gallavotti–Cohen fluctuation relation to thermostated steady states near equilibrium *Phys. Rev.* E **71** 056120
[6] Li B, Casati G and Wang J 2003 Heat conductivity in linear mixing systems *Phys. Rev.* E **67** 021204
[7] Alonso D, Ruiz A and de Vega I 2004 Transport in polygonal billiards *Physica* D **187** 184
[8] Artuso R, Casati G and Guarneri I 1997 Numerical study on ergodic properties of triangular billiards *Phys. Rev.* E **55** 6384
[9] Casati G and Prosen T 1999 Mixing properties of triangular billiards *Phys. Rev. Lett.* **83** 4729
[10] Gutkin E 2003 Billiard dynamics: a survey with the emphasis on open problems *Regular Chaotic Dyn.* **8** 1
[11] Artuso R and Cristadoro G 2003 Weak chaos and anomalous transport: a deterministic approach *Commun. Nonlinear Sci. Numer. Simul.* **8** 137
[12] Artuso R 1997 Anomalous diffusion in classical dynamical systems *Phys. Rep.* **290** 37–47
[13] Gutkin E 1986 Billiards in polygons *Physica* D **19** 311
[14] Galerpin G, Krüger T and Troubetzkoy S 1995 Local instability of orbits in polygonal and polyhedral billiards *Commun. Math. Phys.* **169** 463
[15] Cecconi F, del Castillo-Negrete D, Falcioni M and Vulpiani A 2003 The origin of diffusion: the case of non-chaotic systems *Physica* D **180** 129
[16] Dettmann C P, Cohen E G D and van Beijeren H 1999 Microscopic chaos from brownian motion? *Nature* **401** 875
[17] Lepri S, Rondoni L and Benettin G 2000 The Gallavotti–Cohen fluctuation theorem for a nonchaotic model *J. Stat. Phys.* **99** 857
[18] Benettin G and Rondoni L 2001 A new model for the transport of particles in a thermostated system *Math. Phys. Electron. J.* **7** 3
[19] Jepps O G, Bhatia S K and Searles D J 2003 Wall mediated transport in confined spaces: exact theory *Phys. Rev. Lett.* **91** 126102

[20] Sanders D P and Larralde Hernán 2005 Occurrence of normal and anomalous diffusion in polygonal billiard channels *Preprint* cond-mat/0510654
[21] Troubetzkoy S 1998 Complexity lower bounds for polygonal billiards *Chaos* **8** 242
[22] Gutkin E and Tabachnikov S 2004 Complexity of piecewise convex transformations, with applications to polygonal billiards *Preprint* math.DS/0412335
[23] Lloyd J, Niemeyer M, Rondoni L and Morriss G P 1995 The nonequilibrium Lorentz gas *Chaos* **5** 536
[24] Harayama T, Klages R and Gaspard P 2002 Deterministic diffusion in flower shape billiards *Phys. Rev.* E **66** 026211
[25] Koza Z 2004 Fractal dimension of transport coefficients in a deterministic dynamical system *J. Phys. A: Math. Gen.* **37** 10859–77
[26] Klages R and Dorfman J R 1995 Simple maps with fractal diffusion coefficients *Phys. Rev. Lett.* **74** 387–90
[27] Klages R and Dellago Ch 2000 Density-dependent diffusion in the periodic Lorentz gas *J. Stat. Phys.* **101** 145–59
[28] Chernov N I, Eyink G L, Lebowitz J L and Sinai Ya G 1993 Steady state electric conductivity in the periodic Lorentz gas *Commun. Math. Phys.* **154** 569
[29] Chernov N I, Eylink G L, Lebowitz J L and Sinai Ya G 1993 Derivation of Ohm's law in a deterministic mechanical model *Phys. Rev. Lett.* **70** 2209–12
[30] Chernov N 2001 Sinai billiards under small external forces *Ann. Henri Poincaré* **2** 197–236
[31] Sotta P, Lesne A and Victor J M 2000 The coil–globule transition for a polymer chain confined in a tube: a Monte Carlo simulation *J. Chem. Phys.* **113** 6966–73
[32] Gutkin E 1996 Billiards in polygons: survey of recent results *J. Stat. Phys.* **83** 7
[33] de Groot S R and Mazur P 1984 *Non-Equilibrium Thermodynamics* (New York: Dover)
[34] Chapman S and Cowling T G 1970 *The Mathematical Theory of Non-Uniform Gases* (Cambridge: Cambridge University Press)
[35] Falcioni M and Vulpiani A 2004 private communication
[36] Boffetta G, Cencini M, Falcioni M and Vulpiani A 2002 Predictability: a way to characterize complexity *Phys. Rep.* **356** 367
[37] Korabel N and Klages R 2002 Fractal structures of normal and anomalous diffusion in nonlinear nonhyperbolic dynamical systems *Phys. Rev. Lett.* **89** 214102
[38] Ott Edward 1993 *Chaos in Dynamical Systems* (Cambridge: Cambridge University Press)
[39] Fermi E 1956 *Thermodynamics* (New York: Dover)
[40] Reichl L E 1984 *A Modern Course in Statistical Physics* (Austin, TX: University of Texas Press)
[41] Kittel C and Kroemer H 1980 *Thermal Physics* (San Francisco: Freeman)
[42] Cohen E G D and Rondoni L 2002 Particles, maps and irreversible thermodynamics *Physica* A **306** 117
[43] Rondoni L and Cohen E G D 2002 On some derivations of irreversible thermodynamics from dynamical systems theory *Physica* D **168–169** 341